Computer Aided Geometric Design 102 (2023) 102188

Contents lists available at ScienceDirect

Computer Aided Geometric Design

journal homepage: www.elsevier.com/locate/cagd

# $G^1$ interpolation of $v$-asymmetric data with arc-length constraints by Pythagorean-hodograph cubic splines ☆,☆☆

Yong-Xia Hao *, Wen-Qing Fei

*School of Mathematical Sciences, Jiangsu University, Zhenjiang, 212000, China*

ARTICLE INFO

*Article history:*
Received 19 September 2022
Received in revised form 12 March 2023
Accepted 20 March 2023
Available online 24 March 2023

*Keywords:*
PH cubic spline
Rectifying control polygon
$v$-asymmetric Hermite interpolation
Arc-length constraint

ABSTRACT

The interpolation problem of a sequence of points with prescribed segment arc-length by PH cubic spline is addressed. It turns out to be a $v$-asymmetric $G^1$ Hermite interpolation problem with specified arc length. Using rectifying control polygon and reduction to a canonical form, it is shown that the problem can be expressed in terms of finding the real solutions to a system of nonlinear equations in two variables. A detailed and thorough analysis of the resulting system of nonlinear equations and closed form solutions are provided for any given data. It is confirmed that this construction of $G^1$ Hermite interpolants of specified arc length admits at least two formal solutions, both of which have attractive shape properties and some (if any) must be discarded due to undesired looping behavior. The algorithm developed herein offers simple and efficient closed-form solutions to a fundamental constructive geometry problem that avoids the need for iterative numerical methods. Moreover, the algorithm is illustrated by several numerical examples.



## 1. Introduction

Pythagorean-hodograph (PH) curves are a special class of polynomial curves with polynomial speed functions, which were introduced by Farouki and Sakkalis (1990). The distinctive feature of PH curves offers many useful computational advantages over ordinary polynomial parametric curves. For example, PH curves admit rational offsets and exact arc-length computation, and are well-suited to real-time CNC interpolator algorithms. For a more comprehensive treatment of the construction and properties of PH curves, the reader may consult Farouki and Sakkalis (1990).

The problem of Hermite interpolation has been of interest to the PH community since the nineties (see, e.g., Farin (2008); Farouki (2016); Huard et al. (2014); Cigler and Žagar (2022); Farouki and Neff (1995); Jaklič et al. (2014)). In most Hermite interpolation problems, the data-set is symmetric about the boundary points, in the sense that the same type of information such as curvature, velocity and acceleration is attached to each boundary point. For instance, the classic $C^1$ Hermite data-set consists of two points, each with an associated vector. However, in the Morphosense shape recovery problem, it is desired to reconstruct the geometric shape from the knot and the known distances between consecutive sensors, when placed in contact with a physical object Huard et al. (2014). Therefore, the Morphosense shape recovery is not simply a classical

☆ This work is supported by the National Natural Science Foundation of China (No. 11801225).
☆☆ Editor: Carla Manni.
* Corresponding author.
*E-mail address:* yongxiahaoujs@ujs.edu.cn (Y.-X. Hao).

https://doi.org/10.1016/j.cagd.2023.102188
0167-8396/

Hermite interpolation problem, since the tangents of the sensor knots are not known. Instead, only the curvilinear distances between successive sensors are known. For this problem, two alternative $C^2$ PH quintic spline formulations are proposed, interpolating given spatial data subject to prescribed constraints on the arc length of each spline segment Huard et al. (2014). In our paper, we propose a planar $G^1$ solution with arc length preservation based on rectifying control polygon and cubic PH spline curves, with segments that match the arc-length constraints. The concept of specifying PH curves through rectifying control polygons has been introduced in Kim and Moon (2017) and further developed in Moon et al. (2020a,b). These are characterized by a number of control points that reflect the shape freedoms of PH curves of any given degree, and control polygon lengths that coincide with the total arc lengths of those PH curves.

The present study develops a novel approach to construct planar PH cubic curves based on identifying, for a given sequence of points with prescribed segment arc-length, the rectifying control polygon. It turns out to be the interpolation of asymmetric $G^1$ data (the start and end-points, and the starting tangent direction) by planar PH cubics with prescribed arc lengths. Although the interpolation of (some) $G^1$ data is possible by PH cubics, they do not provide any additional free parameters to be used for the interpolation of the arc length. Thus, as two alternatives, one way is to raise the degree of the interpolating polynomial curve such as Huard et al. (2014) where PH quintic curves were used. The generalizations to the quintic spatial curves can be found in Farouki (2019) and to the PH curves of degree 7 for a special type of approximated curves in Farouki et al. (2021). The other way is to interpolate given data by two PH cubics joined together to be a PH cubic biarc such as Cigler and Žagar (2022). Recently, in Knez et al. (2022) the authors have considered the interpolation of two points, two tangent directions and two corresponding curvatures by $G^2$ PH biarc splines of degree seven with the prescribed arc length.

In this paper, we discuss the relaxation to $G^1$ asymmetric interpolation with given arc length. In fact, the asymmetric $C^1$ Hermite interpolation problem has been already successfully solved in Kong et al. (2013) with PH cubics expressed in the complex representation. Relaxing from $C^1$ to $G^1$ end conditions yields one free scalar parameter, which is used to achieve the desired arc length. It is shown below that this construction of $G^1$ asymmetric Hermite interpolants of specified arc length admits several solutions, of which at least two solutions (which do exist) have attractive shape properties, and the other (if any) must be discarded due to undesired looping behavior. The algorithm developed herein offers simple and efficient closed-form solutions with pleasing shape to a fundamental constructive geometry problem that avoids the need for iterative numerical methods.

The plan for the remainder of this paper is as follows. As a preliminary, the basic framework for planar PH curves and the terminologies and properties of the rectifying control polygons obtained in Kim and Moon (2017) are reviewed in Section 2. In Section 3, we discuss the interpolation of a set of points with segment arc-length, introduce the $G^1$ asymmetric data interpolation problem, verify the existence of solutions, and prove the existence of 'good' PH cubic interpolant. In Section 4, we propose an algorithm for computing the solutions and present some numerical examples to illustrate its performance. Finally, Section 5 briefly summarizes the contributions of the present study, and identifies possible directions for further investigation.

## 2. Preliminary

In this section, we briefly review some basic concepts and the rectifying control polygon of a planar PH curve used in the modeling problem.

### 2.1. Planar PH curves

For its simplicity of the representation of planar PH curves, we use the complex notation for planar curves. A point $z = (z_1, z_1)$ in $\mathbb{R}^2$ is identified with the complex number $z = z_1 + iz_2$ in $\mathbb{C}$. Similarly, a planar parametric curve $\mathbf{r} = (x, y)$ can be identified with a complex valued function $\mathbf{r} = x + iy$.

A planar polynomial curve $\mathbf{r} = x + iy$ is called a PH curve if and only if there exist real polynomials $u$ and $v$ which satisfy

$$x' = u^2 - v^2, \quad y' = 2uv.$$

Moreover, $\mathbf{r} = x + iy$ of odd degree is a PH curve if and only if there exists a complex valued polynomial $\mathbf{z}$ such that

$$\mathbf{r}' = \mathbf{z}^2.$$

One may consult Farouki (1994) for the proof of above results.

### 2.2. Rectifying control polygon of a planar PH curve

Since PH curves are a special class of polynomial curves, every PH curve can be expressed as a Bézier curve. However, a slight change of the Bézier polygon makes the curve lose the PH property. This implies that the Bézier control polygon is not appropriate to control a PH curve since it has redundant degrees of freedom. So the rectifying control polygon is proposed in Kim and Moon (2017). A rectifying control polygon of a PH curve has the same number of degrees of freedom

as the PH curve. It interpolates the end points of the PH curve, but not the end tangents. Most importantly, it has the same arc length as the PH curve.

The concept of rectifying control polygon for PH curves is based on the Gauss-Legendre quadrature. The key property of the Gauss-Legendre quadrature

$$I_m = \sum_{k=0}^{m-1} \omega_k f(\tau_k)$$

with $m$ nodes on [0, 1] is that it gives the exact integral if $f$ is a polynomial of degree $\leq 2m-1$, i.e.,

$$\int_0^1 f(t)dt = \sum_{k=0}^{m-1} \omega_k f(\tau_k).$$

Throughout this paper, the nodes and the weights of the Gauss-Legendre quadrature $I_m$ are denoted by $\tau_0, \ldots, \tau_{m-1}$ and $\omega_0, \ldots, \omega_{m-1}$, respectively. The nodes $\tau_k$ and weights $\omega_k$ of the Gauss-Legendre quadrature up to order 5 can be computed algebraically. For example, for the Gauss-Legendre quadrature with 2 node points, the nodes and the weights are $\tau_0 = \frac{1-\sqrt{\frac{1}{3}}}{2}$, $\tau_1 = \frac{1+\sqrt{\frac{1}{3}}}{2}$ and $\omega_0 = \omega_1 = 1$ respectively.

We review definitions and theorems in Kim and Moon (2017); Kong et al. (2013) to fix some related terminologies and notations. Note that $[\mathbf{p}_0\mathbf{p}_1 \cdots \mathbf{p}_m]$ denotes the polygon that connects the points $\mathbf{p}_0, \mathbf{p}_1, \ldots, \mathbf{p}_m$.

**Definition 2.1.** Data-sets $\{\mathbf{p}_0, \mathbf{p}_1, \mathbf{t}_0, \square\}$ and $\{\mathbf{p}_0, \mathbf{p}_1, \square, \mathbf{t}_1\}$ are said to be v-asymmetric when $\mathbf{p}_0$ and $\mathbf{p}_1$ respectively denote the start and end-points, and $\mathbf{t}_0$ and $\mathbf{t}_1$ denote the velocities at $\mathbf{p}_0$ and $\mathbf{p}_1$, where the symbol $\square$ means that the velocity at the corresponding end-point is not given.

**Theorem 2.1.** *Let* $\mathbf{r}$ *be a PH curve of degree* $2n+1$ *with Bézier control points* $\mathbf{b}_0, \ldots, \mathbf{b}_{2n+1}$. *The nodes and the weights of the n-point Gauss-Legendre quadrature are denoted by* $\tau_0, \ldots, \tau_n$ *and* $\omega_0, \ldots, \omega_n$ *respectively. If we define*

$$\mathbf{p}_0 = \mathbf{b}_0, \quad \mathbf{p}_{k+1} = \mathbf{p}_k + \frac{\omega_k}{2}\mathbf{r}'(\tau_k), \quad k = 0, \ldots, n,$$

*then* $[\mathbf{p}_0\mathbf{p}_1 \cdots \mathbf{p}_{n+1}]$ *is a rectifying polygon of* $\mathbf{r}$.

**Theorem 2.2.** *For a given polygon* $[\mathbf{p}_0\mathbf{p}_1 \cdots \mathbf{p}_{n+1}]$ *of* $n+1$ *segments, there exist* $2^n$ *PH curves of degree* $2n+1$ *whose rectifying polygon is* $[\mathbf{p}_0\mathbf{p}_1 \cdots \mathbf{p}_{n+1}]$. *These PH curves can be specified by*

$$\mathbf{r}(0) = \mathbf{p}_0, \quad \mathbf{r}'(t) = \left(\sum_{l=0}^{n} B_l^n(t)\mathbf{z}_l\right)^2,$$

*where* $\mathbf{z}_0, \mathbf{z}_1, \ldots, \mathbf{z}_n$ *are the solution of the linear system*

$$\mathbf{M}_n \begin{pmatrix} \mathbf{z}_0 \\ \mathbf{z}_1 \\ \vdots \\ \mathbf{z}_n \end{pmatrix} = \begin{pmatrix} \pm\sqrt{\frac{2}{\omega_0}\triangle\mathbf{p}_0} \\ \pm\sqrt{\frac{2}{\omega_1}\triangle\mathbf{p}_1} \\ \vdots \\ \pm\sqrt{\frac{2}{\omega_n}\triangle\mathbf{p}_n} \end{pmatrix}$$

*with the Bernstein-Vandermonde matrix*

$$\mathbf{M}_n = \begin{pmatrix} \mathbf{B}_0^n(\tau_0) & \mathbf{B}_1^n(\tau_0) & \ldots & \mathbf{B}_n^n(\tau_0) \\ \mathbf{B}_0^n(\tau_1) & \mathbf{B}_1^n(\tau_1) & \ldots & \mathbf{B}_n^n(\tau_1) \\ \vdots & \vdots & \vdots & \\ \mathbf{B}_0^n(\tau_n) & \mathbf{B}_1^n(\tau_n) & \ldots & \mathbf{B}_n^n(\tau_n) \end{pmatrix}.$$

## 3. Interpolation of points under length constraint

Note that we restrict our attention here to uniformly parameterized splines, i.e., the parameter domain for each spline segment $\mathbf{r}_i(t)$ is $t \in [0, 1]$. This is appropriate to the Morphosense shape reconstruction problem, since the sensors typically have a uniform distribution along its length Cigler and Žagar (2022).

**Problem** : Construct a $G^1$ PH cubic spline interpolating a sequence of points with prescribed arc lengths for each spline segment. More precisely, given points $\mathbf{p}_0, \ldots, \mathbf{p}_N$ and segment arc lengths $L_1, \ldots, L_N$, identify a set of $G^1$ PH cubic segments $\mathbf{r}_1(t), \ldots, \mathbf{r}_N(t)$ defined on $t \in [0, 1]$ such that

$$\mathbf{r}_i(1) = \mathbf{r}_{i+1}(0), \quad i = 1, 2, \ldots, N-1,$$

and

$$\int_0^1 |\mathbf{r}_i'(t)|dt = L_i, \qquad i = 1, 2, \ldots, N,$$

with $\mathbf{r}_1(0) = \mathbf{p}_0$ and $\mathbf{r}_N(1) = \mathbf{p}_N$.

To guarantee the $G^1$ continuity between consecutive PH spline segments $\mathbf{r}_i$ and $\mathbf{r}_{i+1}$, our method is to find each paragraph in turn: once the segment $\mathbf{r}_i$ is found, the next segment $\mathbf{r}_{i+1}$ can be constructed using $\mathbf{r}_i'(1)$. Therefore, in the following, our problem turns into constructing a planar PH cubic curve $\mathbf{r}(t)$, $t \in [0, 1]$ with given end points $\mathbf{p}_0, \mathbf{p}_1$, tangent $\mathbf{t}$ at the start point $\mathbf{p}_0$ and the arc length $L$. Obviously, we now discuss $G^1$ Hermite interpolation problem with $v$-asymmetric data-set $\{\mathbf{p}_0, \mathbf{p}_1, \mathbf{t}, \square\}$ and the prescribed arc length $L$. It has been demonstrated in Kong et al. (2013) that there exist two PH cubics interpolating $C^1$ Hermite $v$-asymmetric data-set $\{\mathbf{p}_0, \mathbf{p}_1, \mathbf{t}, \square\}$. Relaxation from $C^1$ to $G^1$ end conditions yields one free scalar parameter, which is used to achieve the desired arc length.

### 3.1. $G^1$ Hermite interpolation problem with v-asymmetric data-set

To facilitate the analysis, it is convenient to use canonical form data with $\mathbf{p}_0 = -c$, $\mathbf{p}_1 = c$, where $2c = |\mathbf{p}_1 - \mathbf{p}_0|$. The canonical form amounts to adoption of new coordinates (specified by a translation, scaling, and rotation of the original coordinates), that eliminates the end points $\mathbf{p}_0, \mathbf{p}_1$ as input variables, leaving only the tangent direction of $\mathbf{t}$ and the arc length $L$ as free parameters. Once the canonical form interpolation problem is solved, the solution can be mapped back to the original coordinate system.

**Remark 3.1.** Obviously, there is no solution if $L < |\mathbf{p}_1 - \mathbf{p}_0|$, and a trivial straight-line solution if $L = |\mathbf{p}_1 - \mathbf{p}_0|$. It is assumed henceforth that $L > |\mathbf{p}_1 - \mathbf{p}_0|$.

In the following, we discuss the construction of $G^1$ planar PH cubic curve $\mathbf{r}$ interpolating the canonical-form $v$-asymmetric data-set $\{-c, c, \mathbf{t}, \square\}$ with the arc length $L$ by computing corresponding rectifying control polygon $[\mathbf{p}_0\mathbf{p}\mathbf{p}_1]$. Denote

$$\mathbf{p} = x + iy,\ \Delta\mathbf{p}_0 = \mathbf{p} - \mathbf{p}_0,\ \Delta\mathbf{p}_1 = \mathbf{p}_1 - \mathbf{p},\ \angle\mathbf{p}\mathbf{p}_0\mathbf{p}_1 = \theta_0,\ \angle\mathbf{p}\mathbf{p}_1\mathbf{p}_0 = \theta_1,\ \mathbf{t} = t_1 + it_2.$$

According to the characteristics of the rectifying control polygon, we have

$$\mathbf{r}(0) = \mathbf{p}_0, \quad \mathbf{r}(1) = \mathbf{p}_1, \quad |\Delta\mathbf{p}_0| + |\Delta\mathbf{p}_1| = L.$$

Then by the definition, $\mathbf{p}$ lies on the trajectory of the ellipse with $\mathbf{p}_0, \mathbf{p}_1$ as focal points and the length of the major axis equal to $L$. In this paper, we only discuss the case where the focal points are on the $x$-axis, i.e., the ellipse is

$$\frac{x^2}{a^2} + \frac{y^2}{b^2} = 1,$$

where $L = 2a$, $b = \sqrt{a^2 - c^2}$. It can be similarly discussed for the case where the focal points are on the $y$-axis.

In order to better discuss the existence of the point $\mathbf{p}$, we first give the following two propositions, which are preliminary results and will be used in the proof of later existence theorems.

**Proposition 3.1.** *For arbitrary constants $k, a, c$ $(a > c > 0)$, the equation*

$$\sqrt{a^2 - x^2} - \sqrt{3}x - 2c = k(x + \sqrt{3}\sqrt{a^2 - x^2}) \tag{3.1}$$

*has at least one and at most two solutions $x$ in $[-a, a]$.*

**Proof.** Denote

$$f(x) = \sqrt{a^2 - x^2} - \sqrt{3}x - 2c, \quad g(x) = k(x + \sqrt{3}\sqrt{a^2 - x^2}).$$

Then the number of intersections of graphs of these two functions is just the number of solutions of equation (3.1).

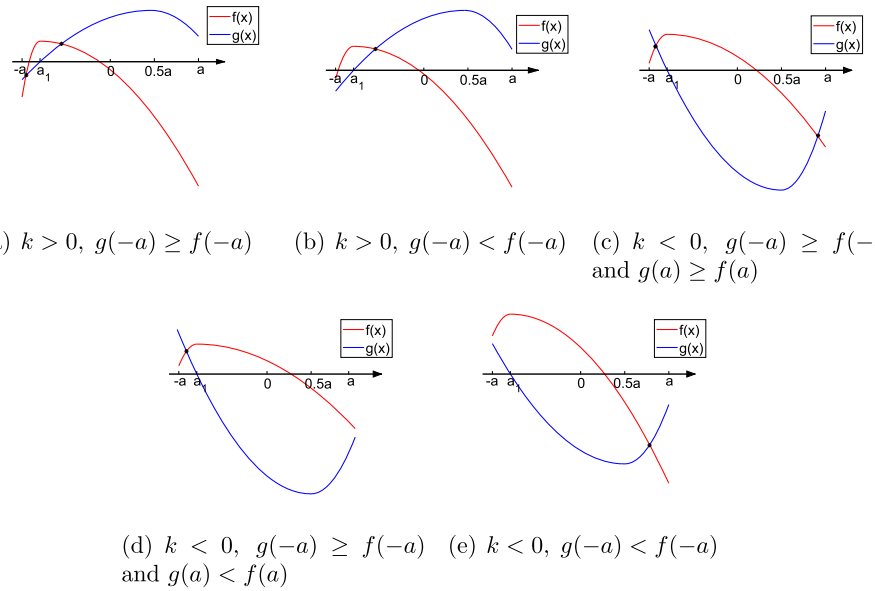


(a) $k > 0,\ g(-a) \geq f(-a)$ (b) $k > 0,\ g(-a) < f(-a)$ (c) $k < 0,\ g(-a) \geq f(-a)$ and $g(a) \geq f(a)$

(d) $k < 0,\ g(-a) \geq f(-a)$ and $g(a) < f(a)$ (e) $k < 0,\ g(-a) < f(-a)$

**Fig. 3.1.** The illustration of Proposition 3.1, where $a_1 = -\frac{\sqrt{3}a}{2}$ is the stationary point of $f$ and $g(a_1) = 0$. (For interpretation of the colors in the figure(s), the reader is referred to the web version of this article.)

On one hand, by taking the derivative of $f$, it can be seen that $f$ increases monotonically on the interval $[-a, -\frac{\sqrt{3}a}{2}]$ and decreases monotonically on the interval $[-\frac{\sqrt{3}a}{2}, a]$. Moreover,

$$f(-a) = \sqrt{3}a - 2c, \quad f\left(-\frac{\sqrt{3}a}{2}\right) = 2a - 2c, \quad f(a) = -\sqrt{3}a - 2c.$$

On the other hand, by taking the derivative of $g$, if $k > 0$, $g$ increases monotonically on the interval $[-a, \frac{a}{2}]$ and decreases monotonically on the interval $[\frac{a}{2}, a]$; if $k < 0$, the situation of increasing and decreasing is the opposite, and

$$g(-a) = -ka, \quad g\left(\frac{a}{2}\right) = 2ka, \quad g(a) = ka.$$

Therefore, according to the shape of these two functions, we have the following three cases:
Case 1: $k > 0$, if $g(-a) \geq f(-a)$, there are two intersection points on $[-a, a]$ for the curves $f$ and $g$; if $g(-a) < f(-a)$, they have only one intersection on the interval $[-a, a]$.
Case 2: $k < 0$, if $g(-a) \geq f(-a)$ and $g(a) \geq f(a)$, they have two intersections on the interval $[-a, a]$; if $g(-a) \geq f(-a)$ and $g(a) < f(a)$ or $g(-a) < f(-a)$, there is only one intersection on the interval $[-a, a]$.
Case 3: $k = 0$, then equation (3.1) becomes $f(x) = 0$. According to the monotonicity of the curve $f$ and $f(-\frac{\sqrt{3}a}{2}) > 0$, $f(a) < 0$, it can be shown that on $[-a, a]$, $f$ has at least one and at most two zeros.
In summary, equation (3.1) has at least one and at most two solutions $x$ in $[-a, a]$. In order to better illustrate these situations, Fig. 3.1 shows the corresponding cases. □

Similar as Proposition 3.1, we also have the following result.

**Proposition 3.2.** *For arbitrary constants $k, a, c$ $(a > c > 0)$, equation*

$$\sqrt{a^2 - x^2} + \sqrt{3}x + 2c = k(x - \sqrt{3}\sqrt{a^2 - x^2}) \tag{3.2}$$

*has at most one solution $x$ in $[-a, a]$.*

According to Theorem 2.2, we have

$$\mathbf{r}'(0) = \mathbf{z}_0^2, \quad \mathbf{r}'(1) = \mathbf{z}_1^2,$$

where

$$\begin{pmatrix} \mathbf{z}_0 \\ \mathbf{z}_1 \end{pmatrix} = \frac{\sqrt{2}}{2} \begin{pmatrix} \pm(1+\sqrt{3})\sqrt{\Delta \mathbf{p}_0} \pm (1-\sqrt{3})\sqrt{\Delta \mathbf{p}_1} \\ \pm(1-\sqrt{3})\sqrt{\Delta \mathbf{p}_0} \pm (1+\sqrt{3})\sqrt{\Delta \mathbf{p}_1} \end{pmatrix}. \tag{3.3}$$

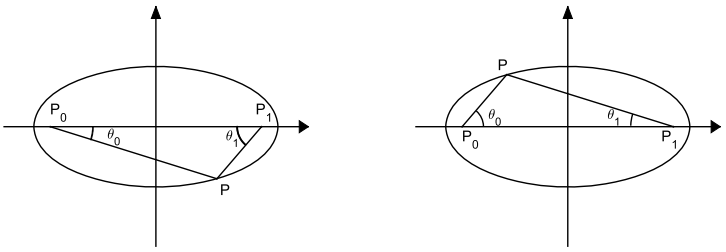


(a) $\mathbf{p}$ located in the lower semi-ellipse (b) $\mathbf{p}$ located in the upper semi-ellipse

**Fig. 3.2.** Illustration of the position of the point $\mathbf{p}$.

Note that a pair of $\mathbf{z}_0, \mathbf{z}_1$ with opposite sign combination has the solutions with opposite sign combination. This pair of solutions produces the same hodograph $\mathbf{r}'$ since $\mathbf{z}$ and $-\mathbf{z}$ produce the same hodograph $\mathbf{r}' = \mathbf{z}^2 = (-\mathbf{z})^2$. So in the following, $\sqrt{\Delta\mathbf{p}_0}$ and $\sqrt{\Delta\mathbf{p}_1}$ denote the square roots having the positive real part of the complex number $\Delta\mathbf{p}_0$ and $\Delta\mathbf{p}_1$ respectively, and we fix the sign of $\sqrt{\Delta\mathbf{p}_0}$ as plus in equation (3.3). Then $\sqrt{\Delta\mathbf{p}_0}$ and $\sqrt{\Delta\mathbf{p}_1}$ have the same sign means they both have the plus sign in equation (3.3), while $\sqrt{\Delta\mathbf{p}_0}$ and $\sqrt{\Delta\mathbf{p}_1}$ have different signs means $\sqrt{\Delta\mathbf{p}_1}$ has the minus sign in (3.3). Then we have the following results.

**Theorem 3.1.** *Let $\mathbf{p} = x + iy$ be located in the lower semi-ellipse. If $\sqrt{\Delta\mathbf{p}_0}$ and $\sqrt{\Delta\mathbf{p}_1}$ have the same sign, there is at least one and at most two PH cubic interpolants to the canonical-form v-asymmetric data-set $\{-c, c, \mathbf{t}, \square\}$ with arc length L. If $\sqrt{\Delta\mathbf{p}_0}$ and $\sqrt{\Delta\mathbf{p}_1}$ have different signs, there exists at most one such PH cubic interpolant.*

**Proof.** If $\mathbf{p}$ is located in the lower semi-ellipse as shown in Fig. 3.2(a), we have

$$\Delta\mathbf{p}_0 = l_0 e^{-i\theta_0}, \quad \Delta\mathbf{p}_1 = l_1 e^{i\theta_1},$$

where

$$l_0 = a + ex, \quad l_1 = a - ex, \quad e = \frac{c}{a}.$$

If $\sqrt{\Delta\mathbf{p}_0}$ and $\sqrt{\Delta\mathbf{p}_1}$ have the same sign, substituting them into the $G^1$ continuity condition $\mathbf{r}'(0) = \mathbf{z}_0^2 = s\mathbf{t} = s(t_1 + it_2)$, we have

$$4c + 2\sqrt{3}x - 2\sqrt{a^2 - x^2} - i\frac{2b}{a}(x + \sqrt{3}\sqrt{a^2 - x^2}) = s(t_1 + it_2), \tag{3.4}$$

where $s$ is a constant. Then, the existence of PH curves satisfying the $v$-asymmetric data-set $\{-c, c, \mathbf{t}, \square\}$ indicates the existence of real solutions $x, s$ to equation (3.4) for arbitrary $t_1, t_2$. Taking the real and imaginary parts, we have

$$\mathrm{T}_1 = 4c + 2\sqrt{3}x - 2\sqrt{a^2 - x^2} = st_1, \ \mathrm{T}_2 = -\frac{2b}{a}(x + \sqrt{3}\sqrt{a^2 - x^2}) = st_2.$$

Case 1: If $t_2 \neq 0$, denote $k = \frac{bt_1}{at_2}$, then we have $\frac{\mathrm{T}_1}{\mathrm{T}_2} = \frac{ka}{b}$, i.e.,

$$\sqrt{a^2 - x^2} - \sqrt{3}x - 2c = k(x + \sqrt{3}\sqrt{a^2 - x^2}).$$

By Proposition 3.1, the above equation has at least one solution and at most two solutions in $[-a, a]$, which means that there exist at least one and at most two PH cubic curves satisfying the requirements.
Case 2: If $t_2 = 0$, we have

$$-\frac{2b}{a}(x + \sqrt{3}\sqrt{a^2 - x^2}) = 0,$$

then $x = -\frac{\sqrt{3}a}{2}$, $s = \dfrac{4c - 4a}{t_1}$. Therefore, there exists one PH cubic curve satisfying the requirements.

If $\sqrt{\Delta\mathbf{p}_0}$ and $\sqrt{\Delta\mathbf{p}_1}$ have different signs, we have

$$4c + 2\sqrt{3}x + 2\sqrt{a^2 - x^2} + i\frac{2b}{a}(x - \sqrt{3}\sqrt{a^2 - x^2}) = s(t_1 + it_2). \tag{3.5}$$

Similarly, taking the real and imaginary parts, we have

$$4c + 2\sqrt{3}x + 2\sqrt{a^2 - x^2} = st_1,\ \frac{2b}{a}(x - \sqrt{3}\sqrt{a^2 - x^2}) = st_2.$$

Case 1: If $t_2 \neq 0$, denote $k = \frac{bt_1}{at_2}$, then

$$\sqrt{a^2 - x^2} + \sqrt{3}x + 2c = k(x - \sqrt{3}\sqrt{a^2 - x^2}).$$

By Proposition 3.2, it has at most one solution in $[-a, a]$, which means that there exist at most one PH curve satisfying the requirements.
Case 2: If $t_2 = 0$, we have

$$\frac{2b}{a}(x - \sqrt{3}\sqrt{a^2 - x^2}) = 0,$$

then $x = \frac{\sqrt{3}a}{2}$, $s = \dfrac{4c + 4a}{t_1}$. Therefore, in this case, there exists one PH curve satisfying the requirements. □

The case when $\mathbf{p}$ is located in the upper semi-ellipse as shown in Fig. 3.2(b) can be discussed similarly and we have the following similar result.

**Theorem 3.2.** *Let $\mathbf{p}$ be located in the upper semi-ellipse. If $\sqrt{\Delta\mathbf{p}_0}$ and $\sqrt{\Delta\mathbf{p}_1}$ have the same sign, there is at least one and at most two PH cubic interpolants to the canonical-form v-asymmetric data-set $\{-c, c, \mathbf{t}, \square\}$ with arc length L. If $\sqrt{\Delta\mathbf{p}_0}$ and $\sqrt{\Delta\mathbf{p}_1}$ have different signs, there exists at most one such PH cubic interpolant.*

### 3.2. Shape analysis

As Theorem 3.1 and Theorem 3.2 state, there exist at least two PH cubic curves satisfying the given $G^1$ Hermite $v$-asymmetric data-set $\{\mathbf{p}_0, \mathbf{p}_1, \mathbf{t}, \square\}$ with prescribed arc length $L$. Now let us discuss the selection problem of the 'best' one among them.

In fact, Moon et al. (2020a) proposed a topological index for quantifying the topological behavior of shapes of PH curves, and a selection criterion of the 'good' solution among the $2^n$ PH curves of degree $2n + 1$ for a given Gauss-Legendre control polygon. By exploiting the lower bound of the absolute hodograph winding number of a PH curve, which is given solely by its type, they presented the existence theorems and demonstrated a good strategy to select PH curves of the zero type as the best PH curve among $2^n$ PH curves. This strategy always gives the unique PH curve with no loops for a non-degenerate control polygon, and the PH curves of the zero type continuously vary in shape while maintaining their topological characteristic unchanged with small change of their control polygons.

To apply the approach to planar PH curves, we first need to restate definitions and results in Moon et al. (2020a) in terms of complex numbers.

**Definition 3.1.** We say that a polygon $[\mathbf{p}_0\mathbf{p}_1 \cdots \mathbf{p}_{n+1}]$ of $n + 1$ segments is a non-degenerate polygon if $\Delta\mathbf{p}_i$ and $\Delta\mathbf{p}_{i-1}$ are not in opposite directions for all $i = 1, \ldots, n$.

**Definition 3.2.** Let $\mathbf{r}$ be a PH curve of degree $2n + 1$ such that its Gauss-Legendre polygon is non-degenerate. Let $\mathbf{z}$ be a complex-valued polynomial of degree $n$ such that $\mathbf{r}' = \mathbf{z}^2$. For $i = 1, \ldots, n$, let $a_i = 0$ if $|\mathbf{z}(\tau_i) - \mathbf{z}(\tau_{i-1})| < |\mathbf{z}(\tau_i) + \mathbf{z}(\tau_{i-1})|$, or equivalently if $|\mathrm{Arg}(\frac{\mathbf{z}(\tau_i)}{\mathbf{z}(\tau_{i-1})})| < \frac{\pi}{2}$, and $a_i = 1$ otherwise. We call the sequence $[a_1, \cdots, a_n]$ of $n$ zero/one binary values the type of $\mathbf{z}$, and also the type of $\mathbf{r}$.

Based on Definition 3.2, for any non-degenerate Gauss-Legendre control polygon of cubic PH curves, Moon et al. (2020a) proved that the PH cubic curve of the zero type is the 'best' one that has no loops with zero absolute hodograph winding number. According to this result, it can be demonstrated that the solution PH cubics when $\sqrt{\Delta\mathbf{p}_0}$ and $\sqrt{\Delta\mathbf{p}_1}$ have the same sign in Theorem 3.1 and Theorem 3.2 belong to the zero type and have good shape with no loops.

**Theorem 3.3.** *For a given canonical-form v-asymmetric data-set $\{-c, c, \mathbf{t}, \square\}$ with the prescribed arc length L, the type of the solution curves when $\sqrt{\Delta\mathbf{p}_0}$ and $\sqrt{\Delta\mathbf{p}_1}$ have the same sign is zero.*

**Proof.** For PH cubic curve, we have $\mathbf{r}'(t) = \mathbf{z}^2(t) = (\mathbf{z}_0(1 - t) + \mathbf{z}_1 t)^2$, and

$$\mathbf{z}(\tau_i) = \mathbf{z}_0(1 - \tau_i) + \mathbf{z}_1\tau_i, \quad i = 0, 1.$$

If $\sqrt{\Delta\mathbf{p}_0}$ and $\sqrt{\Delta\mathbf{p}_1}$ have the same sign, we have

$$\mathbf{z}(\tau_1) - \mathbf{z}(\tau_0) = \sqrt{2}(\sqrt{\Delta\mathbf{p}_0} - \sqrt{\Delta\mathbf{p}_1}), \quad \mathbf{z}(\tau_1) + \mathbf{z}(\tau_0) = \sqrt{2}(\sqrt{\Delta\mathbf{p}_0} + \sqrt{\Delta\mathbf{p}_1}).$$

If $\mathbf{p}$ is located in the lower semi-ellipse as shown in Fig. 3.2(a),

$$\sqrt{\Delta\mathbf{p}_0} = \sqrt{l_0}e^{-i\frac{\theta_0}{2}}, \quad \sqrt{\Delta\mathbf{p_1}} = \sqrt{l_1}e^{i\frac{\theta_1}{2}},$$

then

$$\mathrm{Arg}\left(\frac{\sqrt{\Delta\mathbf{p}_1}}{\sqrt{\Delta\mathbf{p_0}}}\right) = \mathrm{Arg}\left(\sqrt{\frac{l_1}{l_0}}e^{\frac{1}{2}(\theta_0+\theta_1)}\right) = \frac{1}{2}(\theta_0+\theta_1).$$

Since $\theta_0$ and $\theta_1$ are the interior angles of the triangle $\Delta\mathbf{p_0pp}_1$, we have

$$\mathrm{Arg}\left(\frac{\sqrt{\Delta\mathbf{p}_1}}{\sqrt{\Delta\mathbf{p_0}}}\right) < \frac{\pi}{2},$$

which is equivalent to

$$\left|\sqrt{\Delta\mathbf{p}_0} - \sqrt{\Delta\mathbf{p}_1}\right| < \left|\sqrt{\Delta\mathbf{p}_0} + \sqrt{\Delta\mathbf{p}_1}\right|.$$

So $|\mathbf{z}(\tau_1) - \mathbf{z}(\tau_0)| < |\mathbf{z}(\tau_1) + \mathbf{z}(\tau_0)|$. According to Definition 3.2, the type of the solution curve $\mathbf{r}$ is zero.

When $\mathbf{p}$ is located in the lower semi-ellipse, the same result can be obtained similarly. □

By Theorem 3.1, Theorem 3.2 and Theorem 3.3, for a given $v$-asymmetric data-set $\{\mathbf{p}_0, \mathbf{p}_1, \mathbf{t}, \square\}$ with arc length $L$, there exist at least two 'good' $G^1$ Hermite PH cubic interpolants that have no loops.

## 4. Algorithm and computed examples

The following algorithm outline summarizes the procedure for constructing planar PH cubic interpolants to a given $v$-asymmetric data-set $\{\mathbf{p}_0, \mathbf{p}_1, \mathbf{t}, \square\}$ with prescribed arc length $L$.

**Algorithm 1.**

**input**: initial point $\mathbf{p}_0$, final point $\mathbf{p}_1$, tangent $\mathbf{t}$ at the point $\mathbf{p}_0$, and the arc length $L$.

1. set $2c = |\mathbf{p}_1 - \mathbf{p}_0|$, $\theta = \mathrm{Arg}(\mathbf{p}_1 - \mathbf{p}_0)$, $\mathbf{b} = \frac{1}{2}(\mathbf{p}_1 + \mathbf{p}_0)$, $2a = L$, $b = \sqrt{a^2 - c^2}$;
2. convert the original system to a new coordinate system by multiplying $\mathbf{p}_0, \mathbf{p}_1$ by $\cos\theta - i\sin\theta$ and subtracting $\mathbf{b}$, and multiplying $\mathbf{t}$ with $\cos\theta - i\sin\theta$;
3. compute the roots $x$ of the equations (3.4) and (3.5) in closed form when $\mathbf{p}$ is located in the lower semi-ellipse. For the case of upper semi-ellipse, the solutions can be computed similarly;
4. for each computed value $x$, compute the corresponding value $y$ from the equation $\frac{x^2}{a^2} + \frac{y^2}{b^2} = 1$;
5. for each combination of $x$, $y$, form the point $\mathbf{p} = x + iy$;
6. map each point $\mathbf{p}$ to the original coordinate system by multiplying $\mathbf{p}$ with $\cos\theta + i\sin\theta$ and adding $\mathbf{b}$;
7. compute corresponding $\mathbf{z}_0, \mathbf{z}_1$ according to the equation (3.3);
8. compute PH curves $\mathbf{r}$ by $\mathbf{r}(t) = \int_0^t \mathbf{r}'(\tau)d\tau + \mathbf{p}_0 = \int_0^t (\mathbf{z}_0(1-\tau) + \mathbf{z}_1\tau)^2 d\tau + \mathbf{p}_0$.

**output**: planar PH cubic curves $\mathbf{r}$ that satisfy $\mathbf{r}(0) = \mathbf{p}_0$, $\mathbf{r}(1) = \mathbf{p}_1$, $\mathbf{r}'(0) = \mathbf{z}_0^2 = s\mathbf{t}$, $\mathbf{r}'(1) = \mathbf{z}_1^2$, with the prescribed arc length $L$.

The following examples serve to illustrate Algorithm 1 in operation.

**Example 1.** The four formal interpolants to the canonical form data

$$\mathbf{p}_0 = -1, \quad \mathbf{p}_1 = 1, \quad \mathbf{t} = 1 - i, \quad L = 3$$

are shown in Fig. 4.1(a). If $\sqrt{\Delta\mathbf{p}_0}$ and $\sqrt{\Delta\mathbf{p}_1}$ have the same sign and $\mathbf{p}$ is in the lower semi-ellipse, we have two solution values of $\mathbf{p}$ as

$$\mathbf{p}^{[1]} = 0.8472 - 0.9226i, \quad \mathbf{p}^{[2]} = -1.4815 - 0.1751i;$$

when $\mathbf{p}$ is located in the upper semi-ellipse, there exists one solution $\mathbf{p}$ as

$$\mathbf{p}^{[3]} = -0.9442 + 0.8687i.$$

If $\sqrt{\Delta\mathbf{p}_0}$ and $\sqrt{\Delta\mathbf{p}_1}$ have different signs and $\mathbf{p}$ is in the lower semi-ellipse, there exists one control point $\mathbf{p}$ as

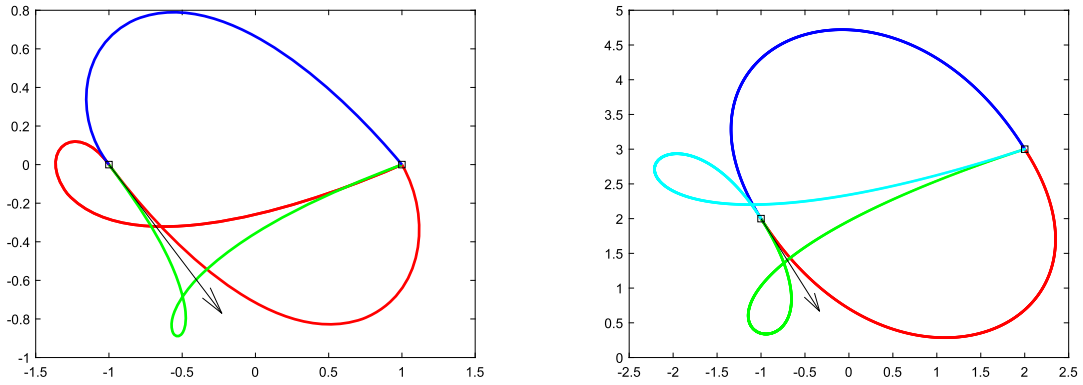

(a) Example 1 (b) Example 2

**Fig. 4.1.** The red, blue, green, and cyan curves represent the interpolants in the lower semi-ellipse with the same sign for $\sqrt{\Delta \mathbf{p}_0}$ and $\sqrt{\Delta \mathbf{p}_1}$, the upper semi-ellipse with the same sign, the lower semi-ellipse with different signs, and the upper semi-ellipse with different signs respectively.

$$\mathbf{p}^{[4]} = -0.6484 - 1.0082i,$$

while there exists no solution when $\mathbf{p}$ is in the upper semi-ellipse. This example illustrates that the solutions when $\sqrt{\Delta \mathbf{p}_0}$ and $\sqrt{\Delta \mathbf{p}_1}$ have the same sign yield smooth curves while the other exhibit an undesirable looping behavior. This behavior is typical of the multiple solutions to PH curve interpolation problems Farouki (2016). The 'good' solutions that have a very pleasing shape are identified as the ones with zero type, which is coincident with Theorem 3.3.

**Example 2.** Consider the $v$-asymmetric data-set

$$\mathbf{p}_0 = -1 + 2i, \quad \mathbf{p}_1 = 2 + 3i, \quad \mathbf{t} = 1 - 2i, \quad L = 6.3198.$$

By Algorithm 1, we first transform it into the new coordinate system with $\mathbf{p}_0^{[1]} = -1.5811$, $\mathbf{p}_1^{[1]} = 1.5811$, then compute the control point $\mathbf{p}$ to get four solutions as

$$\mathbf{p}^{[1]} = 0.4002 - 2.7138i, \quad \mathbf{p}^{[2]} = -0.3756 + 2.7165i,$$
$$\mathbf{p}^{[3]} = -2.5144 - 1.6570i, \quad \mathbf{p}^{[4]} = -2.9049 + 1.0766i.$$

Then convert them into the original coordinates as

$$\mathbf{p}^{[1]} = 1.7379 + 0.0520i, \quad \mathbf{p}^{[2]} = -0.7153 + 4.9583i,$$
$$\mathbf{p}^{[3]} = -1.3614 + 0.1329i, \quad \mathbf{p}^{[4]} = -2.5963 + 2.6028i.$$

Finally, the corresponding PH curves are obtained as shown in Fig. 4.1(b).

As can be seen from above examples, the solution PH cubic curves corresponding to the same sign between $\sqrt{\Delta \mathbf{p}_0}$ and $\sqrt{\Delta \mathbf{p}_1}$ have good shape and free of loops. Moreover, there exist at least two solution curves that yield pleasing shape corresponding to upper and lower semi-ellipse respectively. So in the following problems of blending, we only discuss the $G^1$ blending of this kind 'good' curves.

The next example illustrates the behavior of the two 'good' $G^1$ interpolants with fixed $\mathbf{t}$ and increasing $L$ values.

**Example 3.** Given two end points $\mathbf{p}_0 = 0$, $\mathbf{p}_1 = 1$ and the initial tangent $\mathbf{t} = e^{-\frac{\pi i}{6}}$, Fig. 4.2(a) shows a case in which increasing $L$ values $1.2, 1.3, \ldots, 1.7$ are chosen for the segment, resulting in two kinds radically different 'good' solutions for the curve. It is apparent that the shape varies continuously with the arc lengths.

**Example 4.** This example illustrates the behavior of interpolants with fixed $L$ value and variable $\mathbf{t}$ values. Consider the data $\mathbf{p}_0 = 0$, $\mathbf{p}_1 = 1$, $L = 1.45$ and variable initial tangent

$$\mathbf{t} = e^{-s\pi i}, \quad s = 0, \frac{1}{3}, \frac{1}{2}, \frac{2}{3}, \frac{3}{4}, \frac{4}{5}.$$

Fig. 4.2(b) illustrates the variation of the behavior of the interpolations. This example illustrates the use of the initial tangent as a design parameter.

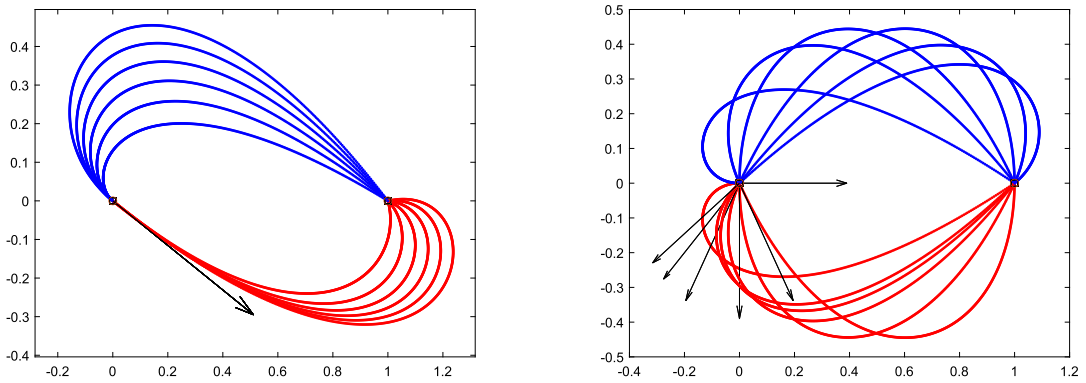

(a) Interpolants with increasing arc lengths (b) Interpolants with variable initial tangent $\mathbf{t}$

**Fig. 4.2.** Example 3 interpolants with increasing length (a) and Example 4 interpolants with variable tangent $\mathbf{t}$ (b).

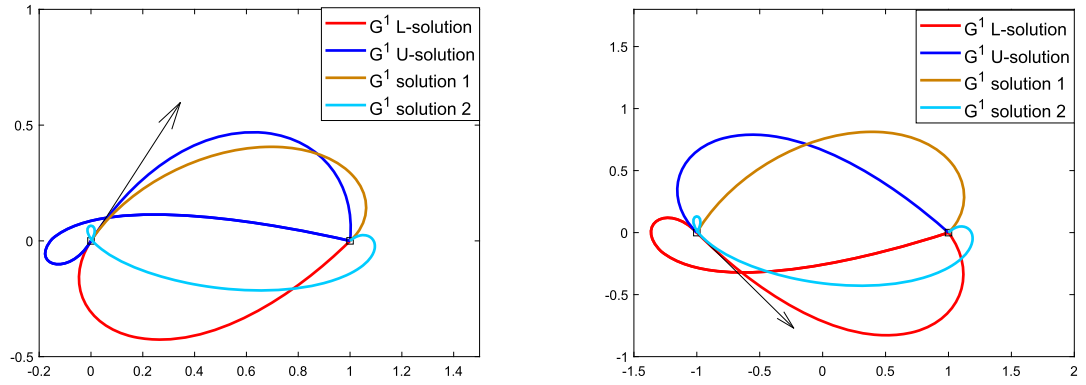


(a) Example 5 (b) Example 1

**Fig. 4.3.** Comparison with the method in Farouki (2016) for Example 5 and Example 1.

The following example is taken from Farouki (2016) used to compare Algorithm 1 with the method in Farouki (2016), where $G^1$ interpolants with prescribed arc length are built using quintic PH curves. Note that the method in Farouki (2016) deals with the symmetric data $\{\mathbf{p}_0, \mathbf{p}_1, \mathbf{t}_0, \mathbf{t}_1\}$, while our method only deals with the $v$-asymmetric data-set $\{\mathbf{p}_0, \mathbf{p}_1, \mathbf{t}_0, \square\}$.

**Example 5.** For comparison, consider the data $\mathbf{p}_0 = 0$, $\mathbf{p}_1 = 1$, $\mathbf{t}_0 = \frac{1}{2} + \frac{\sqrt{3}}{2}i$, $L = 1.5$ and the endpoint tangent vector $\mathbf{t}_1 = -\frac{\sqrt{2}}{2} - \frac{\sqrt{2}}{2}i$. Fig. 4.3(a) illustrates our 'good' $G^1$ PH cubic interpolants and the two quintic interpolants derived by the method in Farouki (2016), where '$G^1$ solution 1', '$G^1$ solution 2', '$G^1$ U-solution' and '$G^1$ L-solution' represent the two $G^1$ PH quintics in Farouki (2016) and our two 'good' $G^1$ interpolants in the upper and lower semi-ellipse respectively. It can be seen that one of the two $G^1$ PH quintic interpolants has undesired shape with loop, just as Farouki (2016) demonstrated. Moreover, the comparison for Example 1 is also presented in Fig. 4.3(b).

Since there exist two PH cubics satisfying the $C^1$ Hermite $v$-asymmetric data-set as demonstrated in Kong et al. (2013), Fig. 4.4 compares the 'good' $G^1$ PH cubic interpolants with prescribed arc length in Examples 1 and 2 with the two $C^1$ cubics having the same end points and tangent direction, where '$C^1$ solution 1' and '$C^1$ solution 2' represent the two $C^1$ PH cubics respectively. Note that it is not possible to impose the arc length constraint on the $C^1$ cubics, and the arc length of two $C^1$ PH cubics for Example 1 and Example 2 is $L = 2.1213$ and $L = 3.6915$ respectively. Moreover, one of the two $C^1$ PH cubic interpolants has undesired shape with loop.

For the Problem, Algorithm 1 is used in above examples to deal with the construction of a single interpolant, i.e., $N = 1$. For the construction of several pieces, the $G^1$ spline interpolants are built as follows: $\mathbf{r}_1$ is constructed firstly with $\{\mathbf{p}_0, \mathbf{p}_1, \mathbf{t}_0, \square\}$ and $L_1$, then construct $\mathbf{r}_2$ by Algorithm 1 with the data $\{\mathbf{p}_1, \mathbf{p}_2, \mathbf{r}_1'(1), \square\}$ and $L_2$, then $\mathbf{r}_3$, and so on until $\mathbf{r}_N$. Finally, the $G^1$ spline interpolants are obtained by joining them together.

**Example 6.** This example compares different 'good' PH cubic interpolants with same given data set $\{\mathbf{p}_i\}_{i=0}^5$, segment arc lengths $\{L_i\}_{i=1}^5$ and initial tangent $\mathbf{t} = 1 - 2i$, where

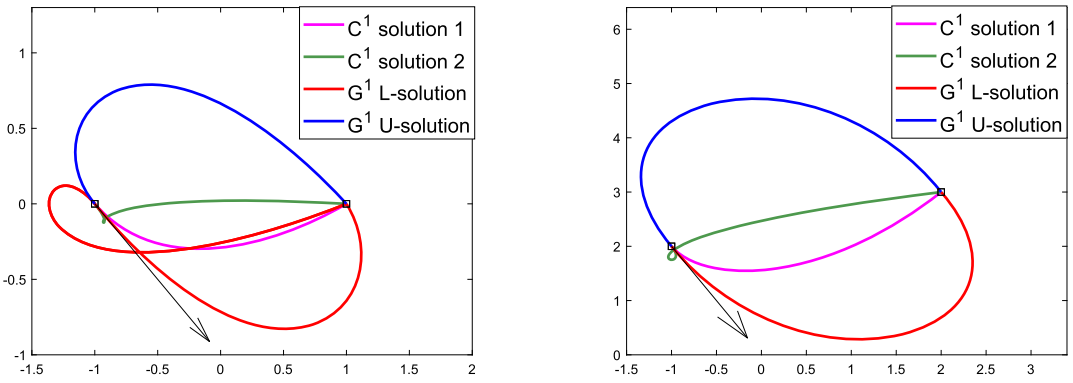


(a) Example 1 (b) Example 2

**Fig. 4.4.** Comparison of the 'good' $G^1$ interpolants with $C^1$ cubics.

**Table 1**
Comparison of the argument of the tangent vector at the nodes for Example 7.

| Nodes | Original | $G^1$ L-solution | $G^1$ U-solution | $C^1$ solution 1 | $C^1$ solution 2 |
|---|---|---|---|---|---|
| 0 | $\frac{\pi}{2}$ | $\frac{\pi}{2}$ | $\frac{\pi}{2}$ | $\frac{\pi}{2}$ | $\frac{\pi}{2}$ |
| $\frac{\pi}{4}$ | $\frac{3\pi}{4}$ | 2.348 | 1.826 | 2.192 | 1.943 |
| $\frac{\pi}{2}$ | $\pi$ | 3.126 | 2.6 | 2.782 | −0.967 |
| $\frac{3\pi}{4}$ | $-\frac{3\pi}{4}$ | −2.378 | −2.898 | −2.300 | 2.486 |
| $\pi$ | $-\frac{\pi}{2}$ | −1.598 | −2.112 | −1.132 | −0.606 |
| $\frac{5\pi}{4}$ | $-\frac{\pi}{4}$ | −0.818 | −1.327 | −1.297 | 2.442 |
| $\frac{3\pi}{2}$ | 0 | −0.036 | −0.5416 | −0.273 | 0.011 |
| $\frac{7\pi}{4}$ | $\frac{\pi}{4}$ | 0.747 | 0.2438 | 0.9618 | −2.365 |
| $2\pi$ | $\frac{\pi}{2}$ | 1.530 | 1.029 | 2.091 | 1.555 |

$$\mathbf{p}_0 = i, \quad \mathbf{p}_1 = 2 + 2i, \quad \mathbf{p}_2 = 4, \quad \mathbf{p}_3 = 5 - i, \quad \mathbf{p}_4 = 6 - i, \quad \mathbf{p}_5 = 8 - 2i,$$
$$L_1 = 3.3045, \quad L_2 = 4.1137, \quad L_3 = 2.1819, \quad L_4 = 1.6160, \quad L_5 = 3.3045.$$

Fig. 4.5 presents the comparison of four combinations of our 'good' segment solution curve and the four combinations of the $C^1$ PH cubic interpolants Kong et al. (2013) having the same end points and initial tangent direction. In the figure, '$G^1$ L-U solution' denotes the spline solution obtained alternately by $G^1$ L-solution first and then $G^1$ U-solution, similarly we have '$G^1$ U-L solution', '$G^1$ L-L solution' and '$G^1$ U-U solution', while '$C^1$ 1-2 solution' represents the spline solution obtained alternately by $C^1$ solution 1 first and then $C^1$ solution 2, similar for '$C^1$ 2-1 solution', '$C^1$ 1-1 solution' and '$C^1$ 2-2 solution'. Obviously, since both $C^1$ cubic PH interpolants can not preserve arc length, the four combinations of $C^1$ PH interpolants have undesirable shape with self-intersections and loops, while the $G^1$ one in Fig. 4.5(c) exhibits better overall shape with milder curvature variations for prescribed data.

**Example 7.** Consider the data $\mathbf{p}_i = \mathbf{r}(s_i)$ from a circular curve

$$\mathbf{r}(s) = 2\cos s + 2i \sin s$$

with $s_i = \frac{i\pi}{4}$, $i = 0, 1, \ldots, 8$, $L_i = \frac{\pi}{2}$, $i = 1, 2, \ldots, 8$ and the initial tangent $\mathbf{t} = 1$. Obviously, the circular curve is divided into eight segments. Fig. 4.6(a) and Fig. 4.6(b) show the two 'good' $G^1$ solutions in this case, while Fig. 4.6(d)-(e) present the two $C^1$ Hermite PH cubic interpolants with the same end points. The curvature plots are also presented in Fig. 4.6(c) and Fig. 4.6(f) for comparison. Moreover, comparison of the argument of the tangent vector at the nodes for these spline solutions with the circular curve $\mathbf{r}$ is given in Table 1. As usual with such comparisons, the $G^1$ solution in Fig. 4.6(a) with the arc length constraint exhibit better overall shape and basically coincides with the original curve.

In Example 7, the data points $\{\mathbf{p}_i\}$, segment lengths $\{L_i\}$ and the initial tangent $\mathbf{t}$ come from a real curve. The data are therefore physically and geometrically coherent, and the interpolation scheme corresponds to a reconstruction problem that aims to find a solution close to the physical curve. Such initial data may, for instance, be obtained by a physical shape sensing system similar to the Morphosense ribbon. Inspired by above example, we try to apply this method to the interpolation of some commonly special curves.

**Example 8.** Consider the data $\mathbf{p}_i = \mathbf{r}(s_i)$ from the cycloid

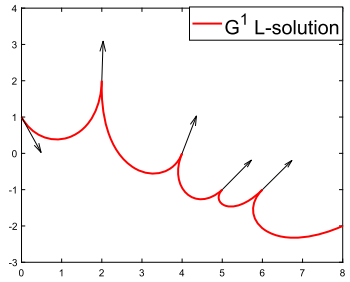


(a) $G^1$ L-L solution

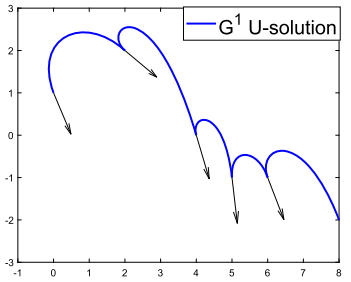


(b) $G^1$ U-U solution

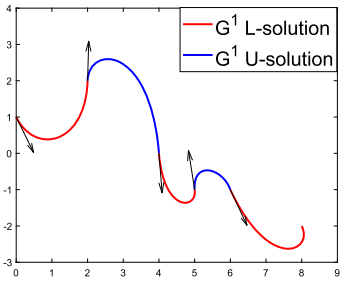


(c) $G^1$ L-U solution

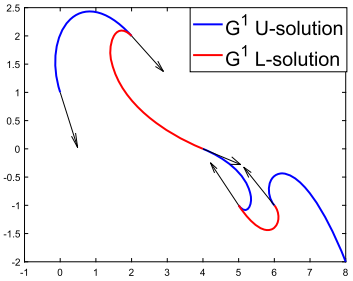


(d) $G^1$ U-L solution

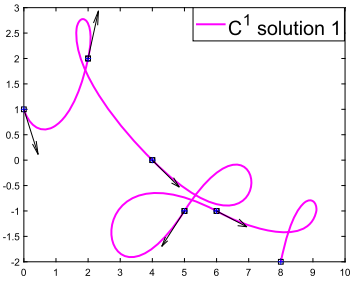


(e) $C^1$ 1-1 solution

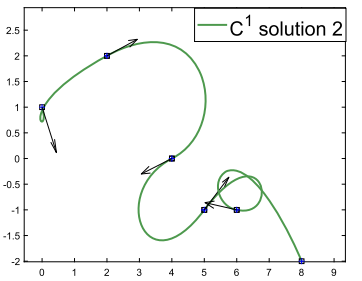


(f) $C^1$ 2-2 solution

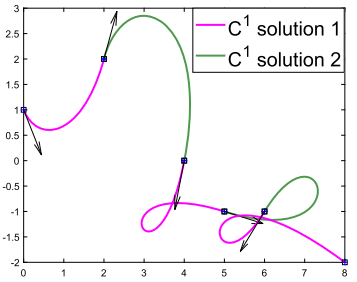


(g) $C^1$ 1-2 solution

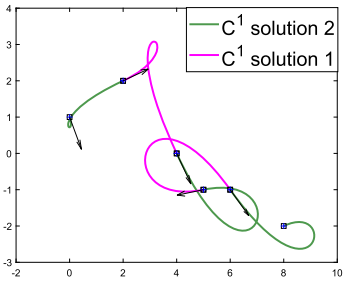


(h) $C^1$ 2-1 solution

**Fig. 4.5.** Spline solutions for Example 6.

$$\mathbf{r}(s) = (\cos s + \frac{\cos ns}{n}) + i(\sin s - \frac{\sin ns}{n})$$

with

$$s_i = \frac{2\pi i}{N},\ i = 0, 1, 2, \ldots, N, \quad L_i = \int_{s_{i-1}}^{s_i} |\mathbf{r}'(s)| ds,\ i = 1, 2, \ldots, N$$

and initial tangent $\mathbf{t} = i$. Fig. 4.7 shows the $G^1$ blending effect for three different kinds cycloid curves and corresponding curvature plots. Moreover, comparison of the argument of the tangent vector at the nodes for the spline solution with $n = 6$, $N = 14$ and the cycloid $\mathbf{r}$ is given in Table 2. As evident in Fig. 4.7, the method can provide a $G^1$ spline curve close to the original curve when using the actual lengths between the knots.

Similarly, we can also consider the $v$-asymmetric data-set from the cardioid

$$\mathbf{r}(s) = (4\sin s + 2\sin 2s) + i(4\cos s + 2\cos 2s)$$

and quadrifolium

$$\mathbf{r}(s) = (5\sin 2s\cos s) + i(5\sin 2s\sin s)$$

respectively with

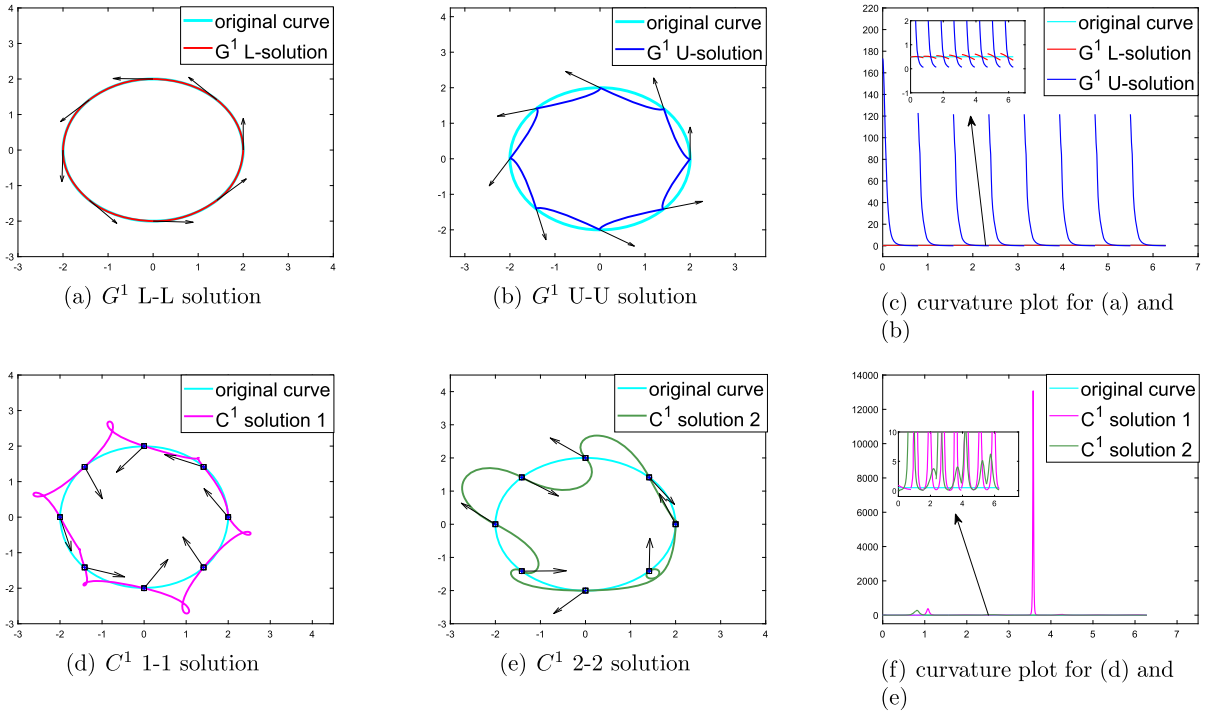


(a) $G^1$ L-L solution (b) $G^1$ U-U solution (c) curvature plot for (a) and (b)

(d) $C^1$ 1-1 solution (e) $C^1$ 2-2 solution (f) curvature plot for (d) and (e)

**Fig. 4.6.** Spline solutions and curvature plots for Example 7.

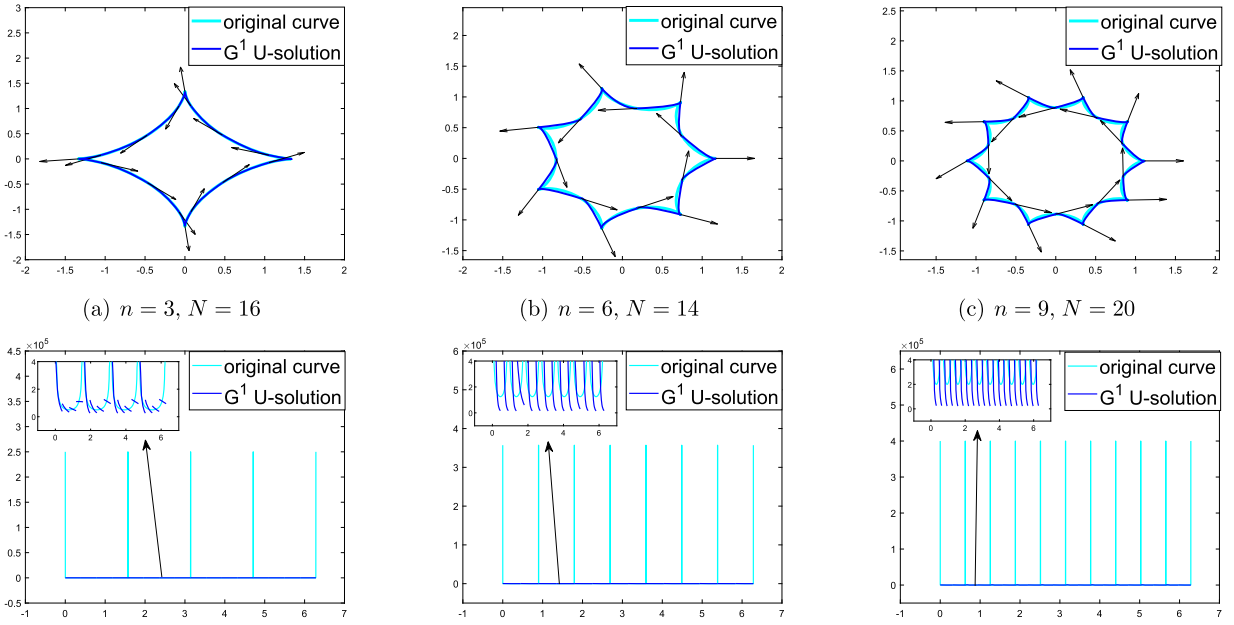


(a) $n = 3$, $N = 16$ (b) $n = 6$, $N = 14$ (c) $n = 9$, $N = 20$

(d) curvature plot of (a) (e) curvature plot of (b) (f) curvature plot of (c)

**Fig. 4.7.** $G^1$ U-U solutions and curvature plots of Example 8 for different $n$ and $N$.

$$\mathbf{t} = \mathbf{r}'(0),\ s_i = \frac{2\pi i}{N},\ i = 0, 1, 2, \ldots, N, \quad L_i = \int_{s_{i-1}}^{s_i} |\mathbf{r}'(s)| ds,\ i = 1, 2, \ldots, N.$$

Fig. 4.8 and 4.9 show the corresponding good interpolants respectively for different point number $N$, which are indistinguishable from the corresponding exact curves on the scale of the plot as $N$ increases.

**Table 2**
Comparison of the argument of the tangent vector at the nodes for Example 8 with $n = 6$, $N = 14$.

| Nodes | Original curve | $G^1$ U-solution |
|---|---|---|
| 0 | 0 | 0 |
| $\frac{\pi}{7}$ | 2.020 | 2.288 |
| $\frac{2\pi}{7}$ | 0 | 1.473 |
| $\frac{3\pi}{7}$ | 2.917 | −3.081 |
| $\frac{4\pi}{7}$ | 0 | 2.187 |
| $\frac{5\pi}{7}$ | −2.468 | −2.189 |
| $\frac{6\pi}{7}$ | 0 | −3.013 |
| $\pi$ | −1.571 | −1.285 |
| $\frac{8\pi}{7}$ | 0 | −2.115 |
| $\frac{9\pi}{7}$ | −0.673 | −0.388 |
| $\frac{10\pi}{7}$ | 0 | −1.218 |
| $\frac{11\pi}{7}$ | 0.224 | 0.405 |
| $\frac{12\pi}{7}$ | 0 | −0.323 |
| $\frac{13\pi}{7}$ | 1.122 | 1.407 |
| $2\pi$ | 0 | 0.577 |

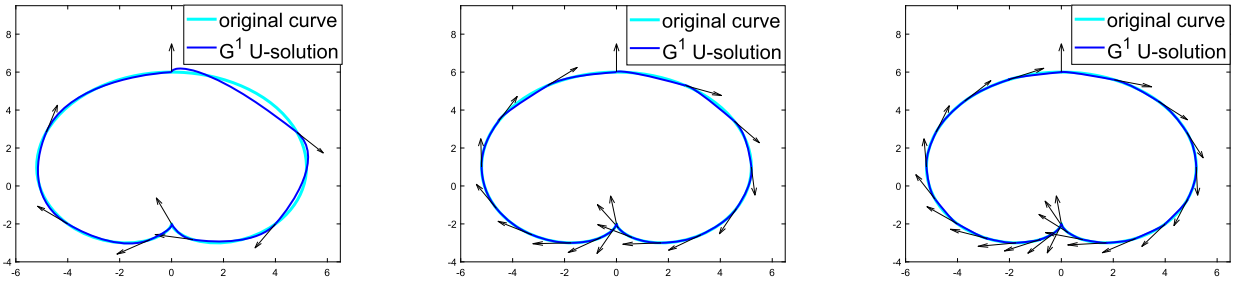


(a) $N = 8$ (b) $N = 18$ (c) $N = 24$

**Fig. 4.8.** $G^1$ U-U solutions of cardioid with different number of points $N$.

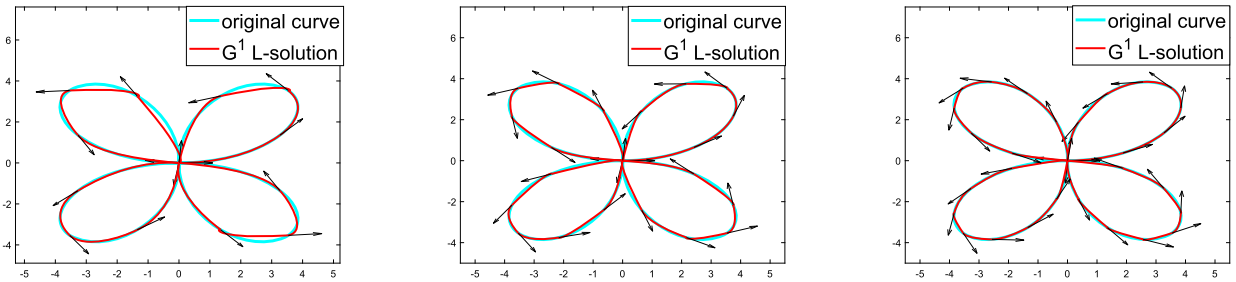


(a) $N = 16$ (b) $N = 24$ (c) $N = 32$

**Fig. 4.9.** $G^1$ L-L solutions of quadrifolium with different number of points $N$.

## 5. Conclusion

Taking advantage of the distinctive properties of rectifying control polygon for PH curves, an elementary and exact solution to the problem of constructing a $G^1$ planar PH cubic spline interpolating a sequence of $\nu$-asymmetric data-set and specified segment arc lengths, has been developed herein. Exploiting the complex PH curve representation, the rectifying control polygon and a reduction of the given data to canonical form, a very simple and efficient algorithm that requires only elementary algebraic computations, is proposed. It has been confirmed that for any appropriate data at least two different solutions exist, both of which have pleasing shape with no loops and can be used to the reconstruction of some special geometric curves.

The present study is only a preliminary investigation into the possibility of interpolating $\nu$-asymmetric data-set with specified arc length by PH curves. It has the virtue of accommodating exact and efficient closed-form solutions that admit very straightforward implementation. As the future work one can consider a similar problem: the interpolation of additional higher order geometric data, such as curvatures. This would either lead to the PH quintic or to PH curves of degree seven.

However, these are analytically and computationally more challenging problems, which are unlikely to admit solutions as simple and exact as obtained in the present context.

## CRediT authorship contribution statement

**Yong-Xia Hao:** Conceptualization, Methodology, Software, Writing – original draft. **Wen-Qing Fei:** Investigation, Software, Writing – review & editing.

## Declaration of competing interest

The authors declare that they have no known competing financial interests or personal relationships that could have appeared to influence the work reported in this paper.

## Data availability

The authors are unable or have chosen not to specify which data has been used.

## References

Cigler, G., Žagar, E., 2022. Interpolation of planar $G^1$ data by Pythagorean-hodograph cubic biarcs with prescribed arc lengths. Comput. Aided Geom. Des. 96, 102119.
Farin, G., 2008. Geometric Hermite interpolation with circular precision. Comput. Aided Des. 40 (4), 476–479.
Farouki, R.T., 1994. The conformal map $z \longrightarrow z^2$ of the hodograph plane. Comput. Aided Geom. Des. 11 (4), 363–390.
Farouki, R.T., 2016. Construction of $G^1$ planar Hermite interpolants with prescribed arc lengths. Comput. Aided Geom. Des. 46, 64–75.
Farouki, R.T., 2019. Existence of Pythagorean-hodograph quintic interpolants to spatial $G^1$ Hermite data with prescribed arc lengths. J. Symb. Comput. 95 (11–12), 202–216.
Farouki, R.T., Neff, C.A., 1995. Hermite interpolation by Pythagorean-hodograph quintics. Math. Comput. 64, 1589–1609.
Farouki, R.T., Sakkalis, T., 1990. Pythagorean hodographs. IBM J. Res. Dev. 34 (5), 736–752.
Farouki, R.T., Pelosi, F., Sampoli, M.L., 2021. Approximation of monotone clothoid segments by degree 7 Pythagorean-hodograph curves. Am. J. Comput. Appl. Math. 382, 113110.
Huard, M., Farouki, R.T., Sprynski, N., Biard, L., 2014. $C^2$ interpolation of spatial data subject to arc-length constraints using Pythagorean-hodograph quintic splines. Graph. Models 76 (1), 30–42.
Jaklič, G., Kozak, J., Krajnc, M., Vitrih, V., Žagar, E., 2014. Interpolation by $G^2$ quintic Pythagorean-hodograph curves. Numer. Math. 7 (3), 374–398.
Kim, S.H., Moon, H.P., 2017. Rectifying control polygon for planar Pythagorean-hodograph curves. Comput. Aided Geom. Des. 54 (5), 1–14.
Knez, M., Pelosi, F., Sampoli, M.L., 2022. Construction of $G^2$ planar Hermite interpolants with prescribed arc lengths. Appl. Math. Comput., 127092.
Kong, J.H., Lee, H.C., Kim, G.I., 2013. $C^1$ Hermite interpolation with PH curves by boundary data modification. Am. J. Comput. Appl. Math. 248, 47–60.
Moon, H.P., Kim, S.H., Kwon, S.H., 2020a. Shape analysis of planar PH curves with the Gauss-Legendre control polygons. Comput. Aided Geom. Des. 82, 101915.
Moon, H.P., Kim, S.H., Kwon, S.H., 2020b. Controlling extremal Pythagorean-hodograph curves by Gauss-Legendre polygons. Comput. Aided Geom. Des. 80, 101852.